J Opt (July 2024) 53(3):1882–1889
https://doi.org/10.1007/s12596-023-01384-7

RESEARCH ARTICLE

Design and simulation of ultra-sensitivity reflective SRI sensor based on TLPFG

Yuxuan Yan[1] · Zhengtian Gu[1,2] · Huiping Jiang[1] · Ying Wang[1] · Jie Du[1]

Received: 27 April 2023 / Accepted: 20 August 2023 / Published online: 19 September 2023

Abstract An ultra-sensitivity reflective surrounding refractive index (SRI) sensor structure based on tilted long-period fiber grating (TLPFG) is proposed in this paper. The sensitivity of the structure to SRI is greatly improved by the combination of the mode transition (MT) region effect and double-peak resonance effect of the high-order cladding mode in TLPFG. A metal mirror is coated at the end of the structure to change the light path and form interference fringes in the reflection spectrum, which greatly reduces the bandwidth of the monitoring peak and makes the measurement more convenient. Firstly, the response characteristics of the effective refractive indices of cladding modes with increasing overlay thickness in MT are analyzed, and a certain grating period is selected to make the TLPFG work at the phase-matching turning point (PMTP) by phase-matching curve (PMC). Then, the parameters of grating angle, grating length and connecting fiber length are optimized by theoretical simulations to make the demodulation more accurate and convenient. On the basis of the above, the reflection spectrum of this structure is simulated, and reflection interference fringes are investigated. Furthermore, the sensing characteristic of SRI of the interference fringes is analyzed. The simulation results show that the average sensitivity can reach 4.86×10^4 nm/RIU when SRI varies in 1.330–1.331, and the highest sensitivity is available to be 9.5×10^4 nm/RIU. In addition, the bandwidth of monitoring peaks of this sensor is 10 times smaller than that of ordinary TLPFG sensors.

Keywords Ultra-sensitivity · Reflective SRI sensor · TLPFG

Introduction

Surrounding refractive index (SRI) is of great significance for pollution monitoring [1, 2], medical diagnosis [3] and marine exploitation [4]. Fiber grating sensors have attracted considerable attention for SRI sensing owing to advantages including resistance to corrosion resistance, electromagnetic interference resistance, ease of multiplexing, remote control, lightweight and low cost [5].

In the past years, a lot of works have been done in order to obtain fiber grating sensors with ultra-sensitivity to SRI. In 1999, Shu et al. first proposed an SRI sensor based on the double-peak resonance effect of LPFG higher-order cladding mode, which has higher sensitivity than sensors based on single-peak resonance [6]. In 2018, Sang et al. demonstrated the effects of grating structure parameters on the transmission spectrum of TLPFG, and pointed out the high-order ($l = 2$) cladding mode has a higher response to SRI [7]. In 2005, Villar et al. proposed the concept of mode transition "(MT)": when the overlay reaches a certain thickness, the high-order mode replaces the low-order mode one by one. From this viewpoint, the resonant wavelength of the cladding mode changes continuously with the overlay thickness [8]. According to literature [6–8], if high refractive index (RI) film is coated on fiber surface based on MT, and the grating period is designed making the high-order cladding mode be in double-peak resonance state. The combination

✉ Zhengtian Gu
zhengtiangu@163.com

[1] Laboratory of Photo-Electric Functional Films, College of Science, University of Shanghai for Science and Technology, 516 Jun Gong Road, Shanghai 200093, China

[2] School of Optical-Electric and Computer Engineering, College of Science, University of Shanghai for Science and Technology, 516 Jun Gong Road, P.O. Box 249, Shanghai 200093, China

of MT effect and double-peak resonance effect of high-order mode in TLPFG will greatly improve the sensitivity of the sensor to SRI. However, literature [9] points out that the sensitivity of the sensor reaches the highest when the grating period is located at the phase-matching turning point (PMTP), but the double-peak resonance will become single-peak resonance at this point, and the bandwidth of the loss peak can reach hundreds of nanometers, which limits the application of sensing. To solve the problem of large bandwidth, Feng et al. proposed to cascade two identical LPFGs, making the transmission spectrum consist of a series of narrow bandwidth loss peaks through interference [10]. However, cascading style will make the sensor structure become larger, and the transmission spectrum monitoring is very inconvenient in the practical application. In 1998, Lee et al. describe self-interference fringes created in a single LPFG formed in a double-cladding fiber, one end of which is coated with a metal film. The interference greatly reduces the bandwidth of the monitoring peaks, making the resolution of monitoring peak greatly improved, and the reflective probe design makes monitoring more convenient [11]. Therefore, assuming that TLPFG is coated with a film of a certain thickness so that the cladding modes are in MT state, the period of TLPFG is located at PMTP. Moreover, a high reflection efficiency metal film is coated on the end face of the grating structure to reflect the optical path. The light coupled into the cladding by TLPFG is reflected and then recoupled back into the core, and it will interfere with the light directly reflected in the core. The combination of MT effect and double-peak resonance effect of high-order mode in TLPFG will greatly improve the sensitivity of the sensor to SRI, and the interference greatly reduces the bandwidth of the monitoring peaks and improves the resolution of monitoring peak; furthermore, the reflective probe design makes monitoring more convenient. Based on this assumption, a reflective sensor structure based on coated TLPFG is proposed in this paper.

Based on the demand for ultra-sensitivity SRI sensor, this paper proposes a reflective sensor structure with coated TLPFG. Then, the parameters of film, grating period, grating length, grating tilt angle and connecting fiber length are optimized by theoretical simulations. The thickness of the high RI film is selected to enhance the sensitivity of the senor based on the MT caused by high RI film; the grating period is chosen from the phase-matching curve (PMC) to make TLPFG operate at PMTP; the length of grating is determined with a function of transmittance and grating length to minimize the transmittance at resonant wavelength; the length of connecting fiber is selected according to the density of interference fringes. Finally, the response characteristic of the loss peak spacing variation to SRI is studied, and the sensitivity of the sensor is calculated. It is found that the sensitivity of this sensor is about 6 times higher than that of the other tilted SRI sensors. The bandwidth of this sensor is about 10 times smaller than that of the other tilted SRI sensors. This study can provide theoretical guidance for the design of ultra-sensitivity SRI sensor.

Theoretical analysis

Structure and coupling mechanisms

The structure diagram of the designed sensor structure is shown in Fig. 1a. It consists of TLPFG, connecting fiber between TLPFG and metal mirror, and metal mirror with lengths of L, d, respectively. The periods of TLPFG are Λ, the RIs of core, cladding, film, and surrounding environment are n_1, n_2, n_3 and n_4, respectively, and a_1, a_2 and a_3 represent the radii of the core, cladding and film, respectively. The TLPFG is with a tilt angle θ and a grating period $\Lambda = \Lambda_g/\cos\theta$.

TLPFG induces only coupling between core mode and codirectional cladding mode in an optical fiber. The coupling characteristics of TLPFG will influence reflection spectrum of the structure. As shown in Fig. 2, the forward core mode is affected by TLPFG and is divided into two parts. One part of the light is coupled from the core to the cladding. This part is reflected back along the original path when it meets the metal mirror, and then coupled back to the core again. The other part of the light propagates in the core and is reflected when it meets the metal mirror, and then returns along the original path. When the light that is reflected back into the core after being coupled into the cladding meets

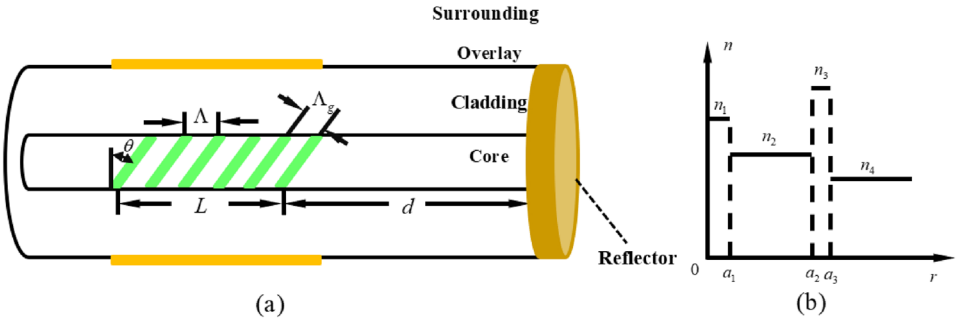

Fig. 1 **a** Structure diagram of the proposed sensor probe; **b** refractive index distribution

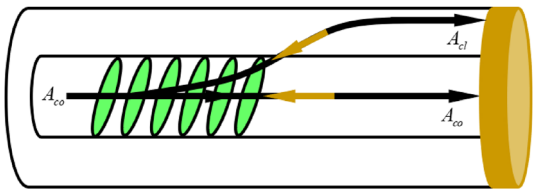

Fig. 2 Coupling paths and corresponding coupling coefficients

with the light that is directly reflected in the core, the second coupling leads to a Michelson interference due to the phase difference of cladding and core modes, and an interference fringe is formed in stop band.

Coupled mode equation

The coupled mode equation of TLPFG can be expressed as [12]:

$$\frac{dA^{\mathrm{co}}}{dz} = \mathrm{if}_{\mathrm{co\text{-}co}}A^{\mathrm{co}} + i\sum_{l,m} g^{+}_{\mathrm{cl,lm\ -\ co}}A^{\mathrm{cl},lm} \times \exp(-2i\delta_{cl,lm-\mathrm{co}}z) \tag{1}$$

$$\sum_{l,m}\left[\frac{dA^{cl,lm}}{dz} = +ig^{-}_{cl,lm-\mathrm{co}}A^{\mathrm{co}} \times \exp(2i\delta_{\mathrm{co}-cl,lm}z)\right], \tag{2}$$

where A^{co} is the amplitude of the core fundamental mode for the transverse mode field traveling to the right ($+z$ direction) and $A^{cl,lm}$ is the amplitude of the νth cladding mode for the transverse mode field traveling to the right ($+z$ direction), and $f_{\mathrm{co\ -\ co}}$ and $g^{\pm}_{cl,lm-co}$ are the self-coupling coefficient of core mode and the cross-coupling coefficient between a specific order cladding mode and core mode. $\delta_{cl,lm-\mathrm{co}}$ and $\delta_{\mathrm{co}-cl,lm}$ are both the small-detuning parameter between core mode and the νth cladding mode, which can be expressed as:

$$\delta_{\mathrm{co}-cl,lm} = \frac{1}{2}\left(\beta^{\mathrm{co}} - \beta^{cl,lm} - \frac{2\pi}{\Lambda_g}\cos\theta\right) \tag{3}$$

Transfer matrix

The transfer matrix of the sensor structure in section i can be expressed as [13]:

$$F_i = \begin{bmatrix} \cos(\gamma l_i) + i\frac{\delta}{\gamma}\sin(\gamma l_i) & i\frac{g^{+}_{cl,lm-co}}{\gamma}\sin(\gamma l_i) \\ i\frac{g^{-}_{cl,lm-\mathrm{co}}}{\gamma}\sin(\gamma l_i) & \cos(\gamma l_i) + i\frac{\delta}{\gamma}\sin(\gamma l_i) \end{bmatrix}, \tag{4}$$

where $\gamma = \sqrt{\left(g^{+}_{cl,lm-\mathrm{co}}\right)^2 + \hat{\sigma}^2}$ and $\hat{\sigma} = \delta_{\mathrm{co}-cl,lm} + (\sigma_{11} + \sigma_{22})/2$[14]. l_i is the length of each uniform grating. $\sigma_{11}(f_{\mathrm{co}-\mathrm{co}})$ is the self-coupling coefficient of core mode. σ_{22} is the mutual coupling coefficient between the cladding modes, which can generally be ignored.

The transfer matrix of the interval fiber in section i can be expressed as follows:

$$F^{c} = \begin{bmatrix} \exp\left[i\pi(n^{\mathrm{co}}_{\mathrm{eff}} - n^{cl,lm}_{\mathrm{eff}})d/\lambda\right] & 0 \\ 0 & \exp\left[-i\pi(n^{\mathrm{co}}_{\mathrm{eff}} - n^{cl,lm}_{\mathrm{eff}})d/\lambda\right] \end{bmatrix}, \tag{5}$$

where $n^{\mathrm{co}}_{\mathrm{eff}}$ and $n^{cl,lm}_{\mathrm{eff}}$ are the effective refractive indices of the core mode and cladding mode at the resonant wavelength, respectively.

The transfer matrix of the whole structure can be described as:

$$F = \begin{bmatrix} t \\ r \end{bmatrix} = F_i \times F^{c} \times \cdots F_{i-1} \times F^{c} \times \cdots F_1 \times \begin{bmatrix} t_0 \\ r_0 \end{bmatrix} \tag{6}$$

where t and r are the amplitudes of the fiber core mode and cladding mode at the tail end of the cascaded grating, respectively. t_0 and r_0 are the amplitudes of the core mode and cladding mode at the beginning of the cascaded grating, respectively. Under the initial condition, $t_0 = 1,\ r_0 = 0$. Finally, the reflectivity of the whole sensor structure can be expressed as:

$$F = \left|\frac{t}{t_0}\right|^2 = t^2 \tag{7}$$

Parameter design

The tilt of TLPFG inspires coupling between the core mode and the cladding mode of azimuthal order $l > 1$. There is little difference in the coupling coefficient between the second-order cladding mode and the first-order cladding mode, but the second-order cladding mode is more sensitive to SRI than the first-order cladding mode[7]. The coupling coefficients for the even cladding modes are much larger than those for the odd cladding modes when azimuthal order $l = 2$, so the order number of odd cladding modes can also be approximately ignored [12]. In order to obtain the highest sensitivity and the best coupling efficiency, the azimuthal order was selected as two and the even cladding mode was chosen.

Film thickness selection

We can effectively improve the response sensitivity of the sensor by coating high refractive index film on fiber surface based on MT [8]. As shown in Fig. 3, the effective refractive indices (ERIs) of the cladding change in the jump-like growth with the film thickness and vary sharply in the film thickness of 240–520 nm and 1580–1860 nm. In MT, the change rate of the ERI of the cladding mode determined the response sensitivity to SRI. The higher the slope is, the more sensitive to SRI the sensor is. In Fig. 3, the dotted line

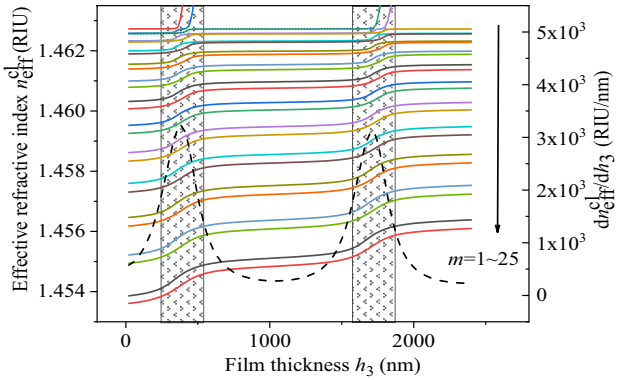

Fig. 3 Relationship between the ERIs of cladding modes and film thickness

indicates the slope of the $m=20$ cladding mode ERI versus film thickness. When the thickness of the film is 380 or 1860 nm, the slope reaches the maximum. It means that this point is the most sensitive to SRI. Considering the cost of actual materials and the complexity of coating, 380 nm is selected as the film thickness.

Grating period selection

In Eq. (3), $\delta_{\mathrm{co}-cl,lm}$ shows the condition for phase matching between the core mode and the νth cladding mode. Thus, the resonant wavelength λ_{res} can be deduced as

$$\lambda_{\mathrm{res}} = \left[n_{\mathrm{eff}}^{\mathrm{co}}(\lambda \mathrm{res}) - n_{\mathrm{eff}}^{cl,lm}(\lambda \mathrm{res})\right]\Lambda. \tag{8}$$

According to Eq. (8), Fig. 4 gives the PMCs of the core modes and high-order cladding modes when the overlay thickness is 380 nm. The curves of the cladding modes ordinal $m=17$–22 shows a quadratic curve. Reference [15] points out that the sensitivity of middle-order cladding mode is higher than low- or high-order cladding mode, and the sensitivity of cladding mode to SRI reaches the maximum when the mode order is 20. For 20th cladding mode, the vertical line has two points (B and C) of intersection with the PMC, which means that the coupling of the core mode to a higher-order cladding mode leads to dual resonant wavelengths. The red-point (A) indicates the point at which the slope of the PMC changes from positive to negative, which is called PMTP. Reference [9] points out that the LPFG in PMTP has the highest sensitivity to SRI. To sum up, the 20th cladding mode was chosen, and the period was selected as 211.64 μm.

Tilted angle and grating length selection

Tilt angle is a vital factor in obtaining an obvious resonance peak in the spectrum. We calculated the mutual coupling coefficient between the order cladding mode ($l=2$) and the core mode in the TLPFG under different tilt angle. As shown in Fig. 5, the mutual coupling coefficient slowly increases until the grating inclination reaches 70°, and it increases sharply after 70°. The mutual coupling coefficient reaches the maximum at 86.5° and decreases rapidly. The magnitude of the coupling coefficient directly affects the strength of the coupling, thus affecting the transmittance. The transmission of the attenuation band is determined by the grating length and the mutual coupling coefficient between the core mode and the cladding mode. It can be expressed as [16]:

$$T(L) = \cos(g_{cl,lm-\mathrm{co}}^{+} L). \tag{9}$$

When the tilt angle is 86.5 degree, the mutual coupling coefficient reaches the maximum, and the transmittance can reach the maximum with the shortest grating length. Therefore, the grating angle of TLPFG was selected as 86.5°.

Figure 6 shows the relationship between transmittance and grating length when the grating at the inclination angle

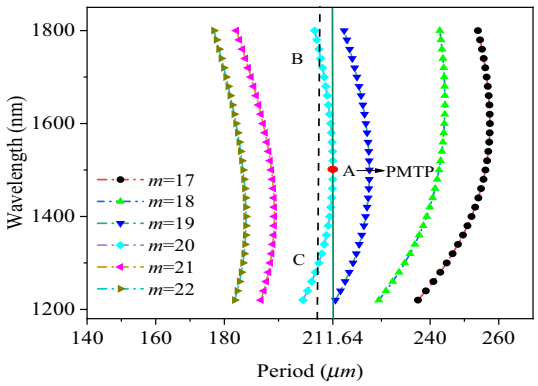

Fig. 4 Phase-matching curves between core modes and higher-order cladding modes

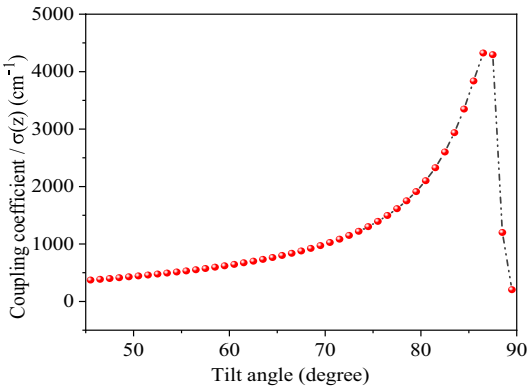

Fig. 5 Coupling coefficient components at different angles based on 20th cladding mode

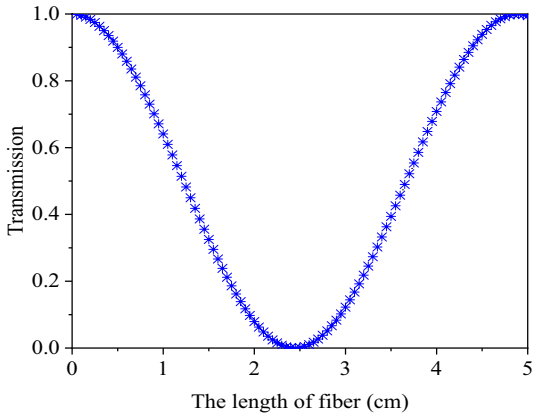

Fig. 6 Relationship between transmittance and grating length

of 86.5°. The transmittance decreases gradually with the increase in grating length, and the grating is in a state of under coupling; when the grating length $L = 2.45$ cm, the transmittance is 0, and the optical power is completely coupled to the cladding. At this grating length, it is in a state of full coupling; while the grating length continues to increase, it will be over-coupled and the transmittance will increase. These three states appear alternately with the increase in grating length. The loss peak in the transmission spectrum is the smallest, and the loss peak is the easiest to detect only when the grating is in the state of full coupling. To sum up, the inclination angle $\theta = 86.5°$and the total grating length $L = 2.45$ cm are selected as the parameters of the theoretical simulation in this paper.

Connecting fiber length selection

Since d is directly connected to the metal mirror, the length of d will directly affect the density of the interference fringes. If the length of d is too short, the interference phenomenon is not obvious. If the length of d is too long, the interference fringes are too dense, which will affect the identification of monitoring peaks. Therefore, an appropriate length of d should be selected. As shown in Fig. 7, the reflection spectra under cascaded fiber lengths are drawn. With the increase in d, the interference fringes become denser.

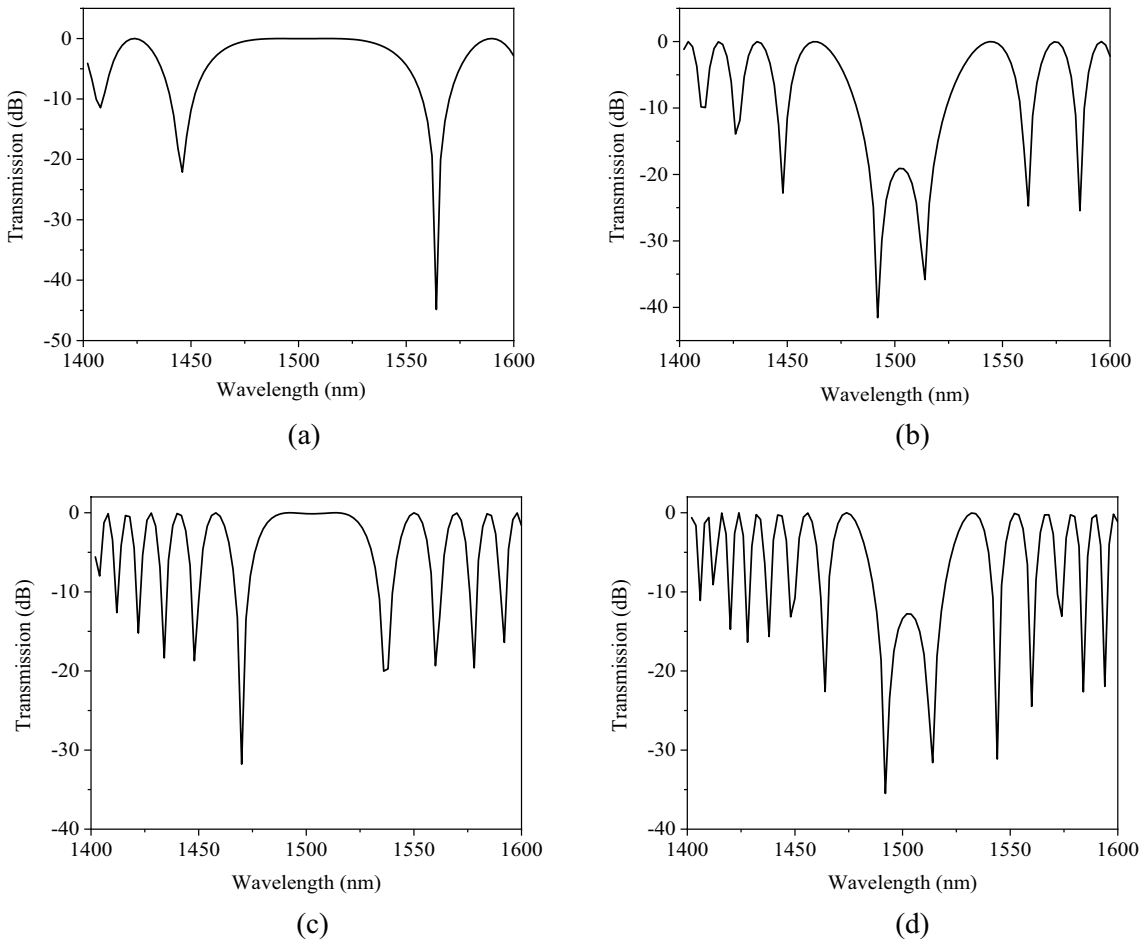

Fig. 7 Reflection spectra under different cascaded fiber lengths **a** $d = 5$ cm; **b** $d = 10$ cm; **c** $d = 15$ cm; **d** $d = 20$ cm

In order to minimize the size of the sensor structure while ensuring that obvious interference fringes can be obtained, $d = 10$ cm is selected. Since the difference of effective refractive index between the higher-order cladding mode and the core mode in TLPFG is smaller than the first-order cladding mode and the core mode in LPFG, a longer cascaded fiber length is required to obtain a significant interference fringe.

Sensing characteristics

Based on the above theoretical analysis, the grating parameters used for simulation are: $a_1 = 2.625$ μm, $a_2 = 62.4$ μm, $n_1 = 1.4580$, $n_2 = 1.45$, $n_3 = 1.57$, $n_4 = 1.33$. TLPFG: $\Lambda = 211.64$ μm, $L = 24.5$ mm, average induced-index change $\sigma_Z = 0.0002$. The thicknesses of the film is 380 nm. The length of the connecting fiber is $d = 10$ cm.

The positions of loss peak are influenced dramatically by the change of the SRIs. The graph is divided into two parts according to the loss peak, with 1500 nm to the left as part A and to the right as part B. The resonance peak of group A moved to the left, and the resonance peak of group B all moved to the right. As shown in Fig. 8, the movement of each loss peak in groups A and B are not identical when SRI changes. Among them, the loss peak near the dividing line has the highest sensitivity. Furthermore, double-peak can further improve the sensitivity, so we choose two loss peaks closest to the dividing line as the two loss peaks of the double-peak.

To investigate the sensitivity of the sensor to SRI better, we obtain the relationship between resonant wavelength and SRI, which is shown in Fig. 9. With the increase in SRI, the resonant wavelength of the loss peak on the left changes 23.6 nm in the short wavelength direction, and the right loss peak moves 25 nm to the long-wave direction. However, the moving rate of the two peaks decreases with the increase in SRI. For double-peak sensing, the wavelength spacing change

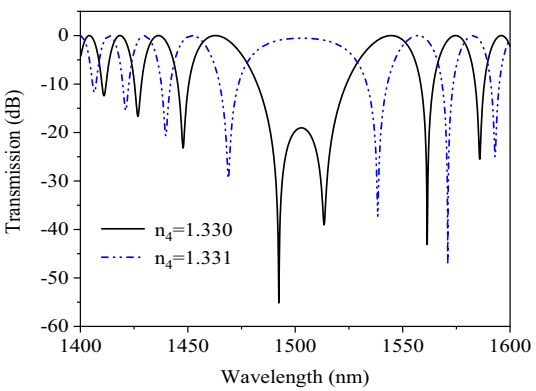

Fig. 8 Reflection spectrum under different SRIs

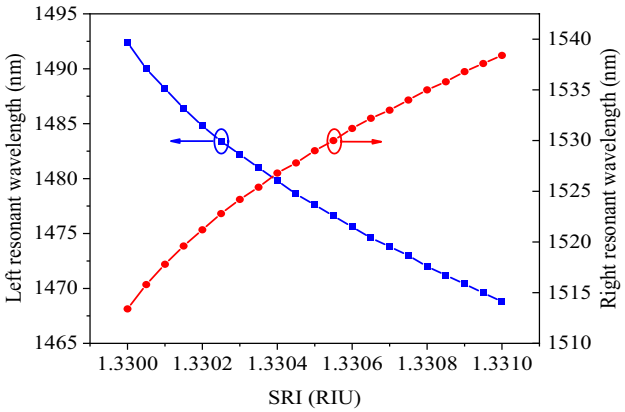

Fig. 9 Resonant wavelengths under different SRIs

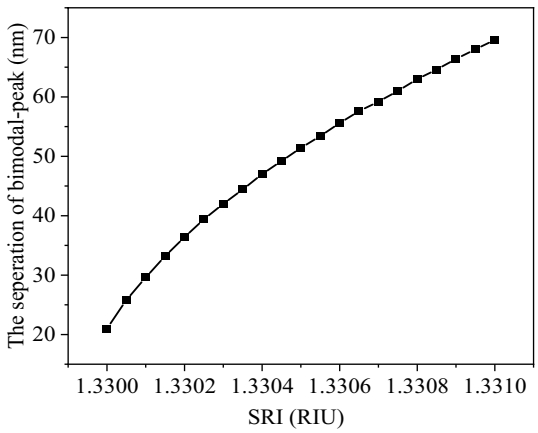

Fig. 10 Dual-peak separation under different SRIs

of the double-peak is the most important parameter. The dependence of the separation of the double-peak on the SRI is presented in Fig. 10. With the SRI changing from 1.330 to 1.331, the wavelength spacing of the two peaks changes from 21 to 69.6 nm. It means a small change in SRI leads to

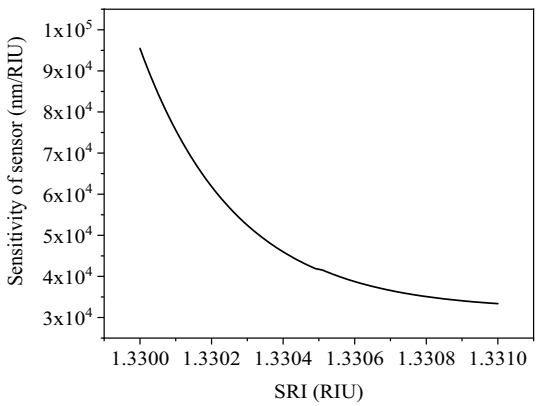

Fig. 11 Sensitivity under different SRIs

Table 1 Comparison with other sensor parameters

Sensors	Detection range (RIU)	Average sensitivity (nm/RIU)	Maximum sensitivity (nm/RIU)	Bandwidth(nm)	Reference
Dual-peak TLPFG sensor	1.35–1.36	1992	1992	47	[7]
Excessively TLPFG	1.33–1.34	8200	12,183	20	[17]
Coated excessively tilted fiber grating	1.330–1.331	23,183	23,183	25	[18]
Reflective sensor structure based on coated TLPFG	1.330–1.331	48,600	95,000	2	This work

a large change in the distance between the two peaks. The SRI sensitivity is up to 4.86×10^4 nm/RIU. The bimodal spacing increases with the increase in SRI, but the increasing rate decreases gradually, that is, the slope decreases. The slope of the curve of bimodal spacing with SRI represents the sensitivity of bimodal sensor to SRI. The smaller the slope is, the lower the sensitivity is.

After obtaining the curve of the separation of double-peak versus SRI in Fig. 10, we further calculate the sensitivity of the sensor to the SRI, which is shown in Fig. 11. We can observe that the sensitivity decreases with the increase in SRI, which is consistent with the previous analysis. When the ambient refractive index is 1.33 and the change of SRI is 1×10^{-5}, the instantaneous sensitivity is as high as 9.5×10^4 nm/RIU, which is the highest sensitivity in the literature that has been read so far. Because the sensor has ultra-high sensitivity in the range of micro refractive index (10^{-5}), it can be used in the field of micro refractive index measurement such as biochemical detection.

In order to highlight the sensitivity advantage of this sensor better, Table 1 lists the sensitivity comparison between this sensor and other tilted sensors and the bandwidth comparison when it is 1/5 away from the lowest transmittance. The sensitivity of the first four sensors selected is the largest in the SRI variation range; however, the sensitivity of the sensor we designed is still about 6 times higher than that of them. The fifth sensor is selected to compare the sensitivity when the SRI changes in the same range, and the highest sensitivity of our sensor is nearly 4 times higher than that of the fifth sensor. The bandwidth comparison results show that the bandwidth of resonant peak is about 10 times smaller than that of other bimodal sensors.

Conclusion

A new reflective ultra-sensitivity SRI sensor based on TLPFG is proposed in this paper. The sensor structure consists of a coated TLPFG and a connecting fiber and a metal film is coated at the end of the structure as a fiber reflector. The high sensitivity characteristic of MT effect and double-peak resonance effect and the narrow bandwidth characteristic caused by MZI interference are fully used. The appropriate parameters of fiber grating are designed according to the coupled-mode theory. By analyzing the relationship between the loss peak of the reflection spectrum and SRI, the sensitivity of the sensor is gained. The results show that the average sensitivity to the SRI is available to be 4.86×10^4 nm/RIU, which is about 6 times higher than traditional TLPFG sensors. The highest sensitivity is available to be 9.5×10^4 nm/RIU, and this is the highest sensitivity in the literature that has been read so far. The bandwidth comparison results show that the bandwidth of this sensor is about 10 times smaller than that of other bimodal sensors. The sensor has excellent characteristics of high sensitivity, reflection measurement and narrow bandwidth, which is expected to be applied in food safety monitoring, biochemical sensing and other fields.

References

1. M. Debliquy et al., Review of the use of the optical fibers for safety applications in tunnels and car parks: pollution monitoring, fire and explosive gas detection. In *Sensing Technology: Current Status and Future Trends III*. ed. by A. Mason, S.C. Mukhopadhyay, K.P. Jayasundera (Springer International Publishing, Cham, 2015), pp.1–24
2. J. Hromadka et al., Multi-parameter measurements using optical fibre long period gratings for indoor air quality monitoring. Sens. Actuators B Chem. **244**, 217–225 (2017)
3. V. Mishra et al., Fiber grating sensors in medicine: Current and emerging applications. Sens. Actuators A **167**(2), 279–290 (2011)
4. R. Min et al., Optical fiber sensing for marine environment and marine structural health monitoring: A review. Opt Laser Technol**140** (2021).
5. L. Wang et al., Overview of Fibre Optic Sensing Technology in the Field of Physical Ocean Observation. Front Phys. **9** (2021).
6. X. Shu, X. Zhu, High sensitivity of dual resonant peaks of long-period fibre grating to surrounding refractive index changes. Electronics Lett **35**(18), 1580–1581 (2019).
7. J. Sang et al. Film sensor based on cascaded tilted long-period and tilted fiber Bragg grating. J Opt **20**(6) (2018).
8. I. Del Villar, et al., Optimization of sensitivity in long period fiber gratings with overlay deposition. Opt Express **13**(1), 56–69 (2005)
9. X. Shu, L. Zhang, I. Bennion, Sensitivity characteristics near the dispersion turning points of long-period fiber gratings in B/Ge codoped fiber. Opt Lett. **26**(22), 1755 (2001).

10. W. Feng, et al. Simulation of novel intensity modulated cascaded coated LPFG sensor based on PMTP. J Opt **19**(12), (2017).
11. B. H. Lee, Temperature sensor using the self-interference of a long-period fiber grating. In: 13th International Conference on Optical Fiber Sensors. Vol. 3746. 1999: SPIE.
12. K.S. Lee, Erdogan, T., Fiber mode coupling in transmissive and reflective tilted fiber gratings. Appl Opt **39**(9), 1394–1404 (2000)
13. T. Erdogan, Cladding mode resonances in short and long period fiber grating filters (vol 14, pg 1760, 1997). J 1Opt Soc Am A.Opt Image Sci Vis **2000**(11), 17 (1997)
14. Z. Xiao-Yun, Zheng-Tian, G.U., Comparison of several sensor models based on long period fiber gratings. Transducer Microsyst Technol **35**(10), 1532–1537 (2008)
15. Z. Zhang, A. Xu, Sensitivity of the thin-clading long period fiber gratings to refractive index. Chin J Sensors Actuators **22**(8), 1105–1108 (2009).
16. O. Duhem et al., Demonstration of long-period-grating efficient couplings with an external medium of a refractive index higher than that of silica. Appl. Opt. **37**(31), 7223–7228 (1998)
17. Z. Li et al., Tuning the resonance of polarization-degenerate LP1, l cladding mode in excessively tilted long period fiber grating for highly sensitive refractive index sensing. J Opt Soc Am A Opt Image Sci Vis **35**(3), 397–405 (2018)
18. Z. Li et al., Titanium dioxide film coated excessively tilted fiber grating for ultra-sensitive refractive index sensor. J. Lightwave Technol. **36**(22), 5285–5297 (2018)